1 Current and Future Climate Compound-Event Flood Impact on
2 Coastal Critical Infrastructures

3 Mariam Khanam[1], Giulia Sofia[1], Marika Koukoula[1], Rehenuma Lazin[1], Efthymios
4 Nikolopoulos[2], Xinyi Shen[1], and Emmanouil Anagnostou[1]

6 [1]Civil and Environmental Engineering, University of Connecticut, Storrs, CT 06269, USA
7 [2]Mechanical and Civil Engineering, Florida Institute of Technology, Melbourne, FL 32901, USA

8 *Correspondence to*: Anagnostou, Emmanouil (emmanouil.anagnostou@uconn.edu)

9 **Abstract.** The changing climate and adverse anthropogenic activities raise the likelihood of damages due to
10 compound flood hazards, triggered by the combined occurrence of extreme precipitation and storm surge during
11 high tides, and exacerbated by sea level rise (SLR). Risk estimates associated with these extreme event scenarios are
12 expected to be significantly higher than estimates derived from a standard evaluation of individual hazards. In this
13 study, we present case studies of compound flood hazards affecting critical infrastructure (CI) in coastal Connecticut
14 (USA) based on actual and synthetic (that is, under future climate conditions) hurricane events, represented by
15 heavy precipitation and surge combined with high tides and SLR conditions. We used the Hydrologic Engineering
16 Center's River Analysis System (HEC-RAS), a two-dimensional hydrodynamic model to simulate the combined
17 coastal and riverine flooding on selected CI sites. We forced a distributed hydrological model (CREST-SVAS) with
18 weather analysis data from the Weather Research and Forecasting (WRF) model for the synthetic events and from
19 the National Land Data Assimilation System (NLDAS) for the actual events, to derive the upstream boundary
20 condition (flood wave) of HEC-RAS. We extracted coastal tide and surge time series for each event from the
21 National Oceanic and Atmospheric Administration (NOAA) to use as the downstream boundary condition of HEC-
22 RAS. The significant outcome of this study represents the evaluation of changes in flood risk for the CI sites for the
23 various compound scenarios (under current and future climate conditions). This approach offers an estimate of the
24 potential impact of compound hazards relative to the 100-year flood maps produced by the Federal Emergency
25 Management Agency (FEMA), which is vital to developing mitigation strategies. In a broader sense, this study
26 provides a framework for assessing risk factors of our modern infrastructure located in vulnerable coastal areas
27 throughout the world.

28 1 Introduction

29 Almost 40 percent of people in the United States live in coastal areas with relatively dense populations (NOAA,
30 2013), where extreme climate events like sea level rise (SLR), storm surges, and inland rainfall play an important
31 role in producing compound flooding and hazards (Wahl et al., 2015; Winsemius et al., 2013; Hallegatte et al., 2013;
32 de Bruijn et al., 2017; de Bruijn et al., 2019). Changes in extreme climate events and the rise of compound flood
33 hazards account for most of the recent increases in damage and economic impacts to society, the environment, and
34 infrastructure (Wahl et al., 2018; Zscheischler et al., 2018), as demonstrated by the combination of unprecedented
35 inland rainfall accumulation and storm surges from hurricanes such as Harvey, Irma, Sandy, and Florence. These

36   events were only the latest in a line of compound events, and they raise concerns about hazards previously

37   considered independent of one another (Barnard et al., 2019; Leonard et al., 2014; Moftakhari et al., 2017; Wahl et

38   al., 2015). When fluvial flooding combines with the co-occurrence of coastal surge and high tide, the potential for

39   extensive inundation is much greater than from either alone, whether in the course of extreme or more frequent

40   events (Moftakhari et al., 2017). SLR induced by climate change will further exacerbate these effects. Continuous

41   economic growth and climate change are expected to increase these severe impacts, as well (Dottori et al., 2018;

42   Blöschl et al., 2017).

43   Concurrent with the rise in disaster event intensities, the damage, and disruption caused by compound coastal events

44   to critical infrastructure (CI) and services, including electrical systems, water, and sewage treatment facilities, and

45   the other utilities that underpin modern society, have substantial adverse socioeconomic impacts. The growing

46   record of significant impacts from extreme events around the world (Chang et al., 2007; McEvoy et al., 2012;

47   Ziervogel et al., 2014; FEMA, 2013; Karagiannis et al., 2017) demands the immediate hardening of critical

48   infrastructure by utilities and governmental agencies to improve system reliability when these major events occur

49   (Pearson et al., 2018). Globally, $2.5 trillion a year is spent on infrastructures meant to perform for decades—a

50   lifespan that will be shortened by the projected effects of climate change (Dawson et al., 2018).

51   A common practice in the study of flooding is a probabilistic analysis of univariate flood drivers (such as

52   streamflow, water level, or precipitation), independent of others. But compound events emerge from complex

53   processes with multiple causes, and they do not conform neatly to traditional categories of extremes or current risk

54   assessment methodologies. On the one hand, tide-surge-SLR are modelled using coastal models in isolated open

55   environments without considering fluvial effects on the flooding. On the other, riverine models cannot capture the

56   risk from tide-surge-SLR effects (Barnard et al., 2017). Consequently, the modelling of individual flood drivers

57   separately mischaracterizes the true risk of flooding to coastal communities and critical infrastructure, introducing

58   uncertainties that make the design of long-lived infrastructure much more difficult. Significant losses can result in

59   when the designs are inadequate and ill-adapted to climate conditions.

60   The impact of climate change on tropical storms and the effects of SLR in coastal areas adds urgency to the need to

61   revaluate management policies based on compound impact, especially on critical infrastructure, to help ensure flood

62   safety and rapid emergency management. Marsooli et al., (2019) suggested the frequency and intensity of coastal

63   flooding induced by hurricanes and tropical cyclones may increase significantly in the twenty-first century. In the

64   past decades, numerous studies have been initiated to find trends in the future intensity and impact of the changes in

65   climate. Recent research has shown spatial variability in SLR and cyclone climatology change results in differences

66   in flood hazards across the basin and global scales (Muis et al., 2016; Marsooli et al., 2019; Vousdoukas et al.,

67   2018).

68   Recent studies have underlined the importance of understanding and quantifying the flood risks to critical

69   infrastructure and their wider impacts on flood risk management and catchment-level planning (Chang et al., 2007;

70   McEvoy et al., 2012; Ziervogel et al., 2014; de Bruijn et al., 2019; Pearson et al., 2018; Pant et al., 2018; Dawson,

71   2018). Few have explored the frequency and risk assessment of compound flooding based on the probability of

72   precipitation and surge (Bevacqua et al., 2019; Wahl et al., 2015), however. The spatial extent and depth of flooding

73   can essentially vary in frequency (Quinn, et al., 2019) from one location to another, and the effects of compound-

74   event flooding (inundation and flood depth) taking into account climate change impact have largely been

75   overlooked. The uncertainty of the current evolution of disaster damage translates into even greater uncertainty

76   concerning future damage to CI. (de Bruijn et al., 2019, Marsooli et al., 2019)

77

78   In this study, we focused on coastal power grid substations as critical infrastructure and investigated the impacts of

79   compound flood hazard scenarios associated with tropical storms. To project the combined hazard, we developed a

80   dynamic framework that investigated climate-driven changes by integrating the effects of SLR, tides, and synthetic

81   future climate hurricane events into flood hazard exposure. This scenario-based analysis provided a comparative

82   flood hazard assessment that allowed us to demonstrate quantitatively the impact of compound flooding on CI in

83   coastal areas and formed the basis on which to address two questions: *(1) How well would critical infrastructure*

84   *weather a hurricane, considering a compound effect of concurrent riverine and coastal flooding during high tides?*

85   *(2) Will future climate (including SLR and intensification of storms due to warmer sea surface temperatures) bring a*

86   *significant increase in flood risk?* We investigated these questions based on eight case studies of CI in the state of

87   Connecticut (USA), distributed on the banks of coastal rivers discharging along the Long Island Sound.

88   **2 Materials and methods**

89   **2.1 Study sites**

90   This study focused on seven coastal river reaches (Fig. 1, Table 1), where eight substations lie in proximity to

91   riverbanks. The critical infrastructure at these sites is prone to flooding caused by both heavy precipitation events

92   and coastal storms (such as hurricanes). For each river reach adjacent to the CI, we developed hydrodynamic model

93   domains, and we applied a hydrological model for predicting river flows from the upstream river basins. Table 1

94   shows the specification of each river reach, drainage basin, the correspondent domain extent for the hydrodynamic

95   simulations, and the hydrological distance of each substation from the coastline. The hydrologic distance represents

96   the distance from each CI to the coastline. This distance is measured along the direction of flows, and it was derived

97   using the 30m National Elevation Dataset (NED) for the continental United States (USGS 2017). The considered

98   rivers belong to watersheds ranging from 10 to 300 km2 in extent. For this study, the simulated domains ranged

99   from 3.7 to 8.3 km in river length and 2.2 and 20.7 km2 in area. The substations were coded from CI1 to CI8.

100   Except for CI4 and CI5, which are within the same simulation domain, each substation has an independent domain.

101   **2.2 Simulation framework**

102   To evaluate the effect of compound events, we selected four tropical storms: two actual hurricanes that hit

103   Connecticut (Sandy and Irene) and two synthetic hurricanes based on actual hurricanes Sandy and Florence. We

104   subjected the latter two events to different atmospheric conditions leading to landfall scenarios with greater impacts,

105   with the Sandy scenario representing hurricane Sandy under future climate atmospheric and sea surface conditions

106   (Lackmann 2015). Both Irene (August 21–28, 2011) and Sandy (October 22–November 2, 2012) reached category 3,

107 but they made landfall in Connecticut as category 1 hurricanes. To investigate the impact of floods under different

108 climate and compound effect scenarios associated with river flows, tides, storm surge, and SLR, we devised a

109 combined hydrological (subsection b, below) and hydrodynamical (subsection c) modeling framework (Figure 2),

110 forced with weather reanalysis data and geospatial data for the actual events and a numerical weather prediction

111 model (subsection a) for the synthetic events (that is, synthetic hurricane Florence and future hurricane Sandy).

2.2.1 Atmospheric simulations

113 To simulate the two synthetic hurricane events, we used the Weather Research and Forecasting (WRF) system

114 (Powers et al., 2017; Skamarock et al., 2007). For synthetic Florence, we used a hurricane track forecast by the

115 National Oceanic and Atmospheric Administration (NOAA) that showed landfall in Long Island and Connecticut,

116 and we based synthetic Sandy on future climate conditions (post 2100). For the soil type and texture input in the

117 WRF model for both synthetic storm simulations, we used USGS GMTED2010 30-arc-second (Danielson and

118 Gesch 2011) DEM for the topography, Noah-modified 21-category IGBP-MODIS (Friedl et al., 2010) for land use

119 and vegetation input, and Hybrid STATSGO/FAO (30-second) (FAO 1991) for soil characteristics.

120 More specifically, as of September 6, 2018, according to the Global Forecast System (GFS) forecasts of the National

121 Centers for Environmental Prediction (NCEP) (Higgins 2000), the prediction for one of the tracks of Florence

122 showed landfall in Long Island and Connecticut on September 14 as a category 1 hurricane. To simulate the

123 synthetic hurricane Florence with WRF, we used these GFS forecasts at 0.25° x 0.25° spatial resolution as initial and

124 boundary conditions. We used a three-grid setup with a coarse external domain of 18 km spatial resolution and two

125 nested domains with 6 km and 2 km horizontal grid spacing, respectively. Two-way nesting was activated for both

126 inner domains. Vertically, the domains stretched up to 50 mb with 28 layers. We parameterized convective activity

127 on the outer (resolution of 18 km) and the first nested (resolution of 6 km) domain using the Grell 3D ensemble

128 scheme (Grell and Devenyi 2002). Further details on the model setup are presented in Table 2.

129 For the future hurricane Sandy scenario, we used the hurricane Sandy simulations under future climate conditions

130 (after 2100) by Lackman (2015), who used a three-grid setup at spatial resolutions of 54, 18, and 6 km. We defined

131 initial and boundary conditions by altering the European Centre for Medium-Range Weather Forecasts (ECMWF)

132 interim reanalysis (Dee et al., 2011) data, based on five General Circulation Model (GCM)-projected, late-century

133 thermodynamic changes derived from the IPCC (Intergovernmental Panel on Climate Change) AR4 A2 emissions

134 scenario (Meehl et al., 2017). A complete description of the modeling framework is provided by Lackman (2015).

2.2.2 Hydrological modelling

136 To account for the river inflow (upstream boundary condition), we devised CREST-SVAS (Coupled Routing and

137 Excess Storage–Soil–Vegetation–Atmosphere–Snow) (Shen and Anagnostou 2017), a physically-based distributed

138 hydrological model. To simulate river discharges for the synthetic hurricanes (Florence and future Sandy), we used

139 the WRF simulations at 6-km/hourly spatiotemporal resolution, as described above. To force the hydrological model

140 for the actual events (Sandy and Irene), we used data from Phase 2 of the North American Land Data Assimilation

141 System (NLDAS-2) (Xia et al., 2012) dataset. NLDAS-2 is a gridded dataset derived from bias-corrected reanalysis

142   and in situ observation data, with a one-eighth-degree grid resolution and an hourly temporal resolution, available
143   from January 1, 1979, to the present day. We derived the precipitation from daily rain gauge data over the
144   continental United States, and all other forcing data came from North American Regional Reanalysis (NARR) by
145   NCEP (Higgins 2000), to which we applied bias and vertical corrections. In CREST-SVAS, we resampled the direct
146   runoff of each grid at 500 m resolution to 30 m routing in coastal basins of the small drainage area (see Table 1) to
147   improve the accuracy of river flow estimation. To reduce the computational effort, we performed the hydrological
148   simulation using a hydrologically conditioned 30 m spatial resolution digital elevation model (DEM) (USGS 2017).
149   Also included in the hydrological model was land use and land cover (LULC) information retrieved from the
150   Moderate Resolution Imaging Spectroradiometer ("MOD12Q1" from MODIS). (Friedl et al., 2015) To compensate
151   for the coarse resolution (500 m) of these data, we obtained imperviousness ratios using Connecticut's Changing
152   Landscape (CCL) database and the National Land Cover Database (NLCD) at 30 m resolution. In CREST-SVAS,
153   the land surface process was simulated by solving the coupled water and energy balances to generate streamflow at
154   hourly time steps at the outlet of the studied watershed. The model has been validated (Shen and Anagnostou, 2017;
155   Hardesty et al., 2018) in river basins within Connecticut, where all the watersheds simulated in this study reside.

2.2.3 Hydrodynamic modelling

157   To assess the flood hazard in terms of extent and the maximum depth, we implemented the Hydrologic Engineering
158   Center's River Analysis System (HEC-RAS), developing individual two-dimensional model domains for each CI
159   location. We generated simulation grids from 1 m LiDAR DEM archived in Connecticut Environmental Conditions
160   Online (CtECO 2016), including building footprints to represent better the impacts of urban establishments on
161   inundation dynamics. To reduce the computation time, we created a 2D mesh grid at 10 m background resolution,
162   enforced with breaklines to intensify the riverbank and other areas with a large elevation gradient up to 1 m
163   resolution. HEC-RAS allowed a gradual mesh distribution around the breaklines, preserving most of the information
164   from the 1 m DEM. For the hydrodynamic model, we retrieved 2011 land cover classification data from the National
165   Land Cover Database (NLCD). The upstream boundary condition was provided by CREST-SVAS, and the
166   downstream boundary condition (coastal water level, including coastal tide, storm surge, and sea level) was derived
167   from National Water Level Observation Network (NWLON) data, provided by NOAA. These data are available as
168   actual observations and predictions at intervals of six minutes to one hour. Figure 3 provides an example of one of
169   the sites, showing the upstream and downstream boundaries, along with a map overlay of flooded areas of five
170   (SD1–SD5) scenarios (see below) for CI2. We initiated the simulation with a warmup period of 12 hours to achieve
171   stability. We chose the full momentum scheme in HEC-RAS and extracted hourly output from the simulation.
172   To validate the hydrodynamic model simulations, we used surveyed HWMs (high water marks) (Koenig et al.,
173   2016) collected by the United States Geological Survey (USGS) after hurricane Sandy at 15 selected locations
174   spread across the simulation domains. HWMs are frequently used to calibrate and validate model outputs and
175   satellite-based observations of flood depth (Bunya et al. ,2010; Cañizares and Irish 2008; Cariolet, 2010; Chang et
176   al., 2007; Hostache et al. 2009; McEvoy et al., 2012; Pearson et al., 2018; Schumann et al., 2008; Schumann et al.,
177   2007; Schumann et al., 2007; Ziervogel et al., 2014).

178 An HWM does not necessarily indicate the maximum flood depth; rather, it can be a mark from a lower depth that

179 lasts long enough to leave a trail. Based on this understanding, we compared the HWMs against the simulated flood

180 depths. The simulated depths demonstrated reasonable agreement with the collected HWM values (Figure 4), with

181 the model tending to show a slight overestimation in all cases. In the current study, this limitation came mostly from

182 the uncertainty in the LiDAR DEMs. LiDAR data, especially in large and deep channels, do not provide a suitable

183 representation of the submerged channel bed, and this results in an underestimation of channel conveyance capacity

184 and subsequent overestimation of the flood extent. In this case, systematic error fell within values of expected

185 precision, implying a consistent positive bias in the simulations not strong enough to hinder the results.

2.3 Compound scenarios

187 We modelled four types of synthetic compound event scenarios besides the simulation of the actual events by (1)

188 simulating the synthetic hurricanes; (2) introducing a climate change factor, in the form of SLR (~0.6 m), as

189 projected for 2050, as a prediction for intermediate low probability (CIRCA 2017); (3) shifting the surge timing to

190 make the high tide coincides with the storm surge; and (4) combining the SLR with the high tide condition. The

191 combination of these four scenario types yielded nine compound scenarios. The following describes the simulated

192 scenarios for the three hurricane events.

193 IR1 and IR2 were the two scenarios for hurricane Irene. IR1 was the actual hurricane Irene, and IR2 was the IR1

194 scenario with future SLR added to the tidal water level at the downstream boundary of HEC-RAS. A point to note is

195 that hurricane Irene made landfall in Connecticut during high tides.

196 For hurricane Sandy, we generated five scenarios. SD1 was the actual Sandy. For SD2, we shifted the tide time

197 series to coincide with the peak surge. SD3 was scenario SD2 with SLR added to the modified total water level from

198 NOAA. The remaining two scenarios for hurricane Sandy represented future climate conditions. Specifically, SD4

199 was the future scenario simulated with the GFS and shifted NOAA tidal water levels. SD5 was the future Sandy

200 with shifted tide and SLR.

201 For the Florence event, we simulated two scenarios. FL1 was the synthetic Florence event, based on the GFS track

202 that gave landfall in Connecticut and Long Island. FL2 was scenario FL1 with SLR added to the coastal water

203 levels.

204 Table 3 shows, for each scenario, the basin-averaged event accumulated precipitation (mm) and the simulated peak

205 flow (m3/s) at the basin outlets, along with the recurrence interval of the peak flows derived from the long-term

206 simulated flows from CREST. We have used the Log- Pearson probability distribution method to fit the annual

207 maximum flows. The flood frequency curves are then used to determine the corresponding recurrence interval of the

208 peak flows for different scenarios. This shows how significant the precipitation was for each considered scenario.

209 For CI1, for example, the future Sandy (SD 4/5) scenario, with a peak flow of 242.4 m3/s, was the most extreme

210 event with a recurrence interval of 316 year, followed by Irene (158.5 m3/s) and Florence (51.3m3/s) with a

211 recurrence interval of 56 and 2 year consecutively, whereas for CI8, Florence and future Sandy had similar

212 magnitudes with peak flows of 93.1m3/s (6) and 94.7m3/s (6), respectively. In table 4, we have summarised the

213 maximum total water level (tide & surge) used in the model at the downstream of the study sites for all the

214 scenarios. This table represents the change in the severity of the coastal component of the compound scenarios
215 concerning added challenges like shifted tide and SLR. For example, for CI3, the total water level increases 1m with
216 the shifted tide (SD2/ SD4) and with SLR it becomes 4.4 m.

2.4 Compound flood hazard analysis

218 We investigated the compound effect of the different events by quantifying flood area extent and flood level
219 differences in the coastal flood hazard estimates. For the flood area extent, we used as a baseline the 100-year flood
220 maps. For the flood level differences, we considered the overall distribution of water depths across the domain of the
221 CI sites and investigated the time series of water depth at each location (Figure 5).

222 Using the time series of flood levels and specified threshold depths, we determined the time periods when flooding
223 exceeded these threshold levels. Specifically, we considered 0.5 m, 1.5 m, and 2.5 m for threshold levels, which
224 represented possible CI levels. For each threshold level, we determined the percentage of time flood in a 24-hour
225 window that inundation was over the threshold (Figure 5; red rectangle). We associated the changes in risk posed to
226 the CI from the different examined scenarios with the changes in those percentages. This analysis indicated as to
227 whether and for how long CI components could be below floodwater.

3 Results and Discussions

3.1 Flood extent

230 We compared the simulated flood extents to the FEMA 100-year flood zone for all the scenarios (Table 4, Figure
231 6a–c). Inundated areas ranged between less than 1 km2, with a minimum extent of 0.4 km2 for the actual Sandy
232 (SD1) at C8, to more than 7 km2, with a maximum extent of 7.1 km2 for the future Sandy (SD5) at C3. Changes
233 across the study sites relative to the FEMA extent ranged from –87.8% (for CI8 for SD1) to 192.2% (for CI2 for
234 IR2). The results showed strong agreement that the flood extents increased with increasing intensity of the events
235 and increase in their recurrence intervals (explained in Table 3). The sites with a return period of fewer than 100
236 years, as expected, showed consistently less flooding than shown on the FEMA map, a finding best represented by
237 the comparison of actual events (IR1 and IR2); for example, as shown in Table 4, the CI1–CI8 for IR1 and SD1 had
238 less inundated areas than shown on the FEMA 100-year flood map, which resonates positively with the return period
239 of the peak flows in Table 3. As we proceeded with the synthetic scenarios, adding compound and future challenges,
240 the results indicated the supplementary impacts of the joint flood drivers (shifted tide, surge, SLR). Therefore, the
241 percentage change was the most useful basis for comparison of the different scenarios of an event.

242 The shift in tide time (SD2) resulted in more flooding than resulted from actual Sandy (SD1). The increase in flood
243 extent ranged from 8.3% (CI4/5) to as high as 425% (CI8), showing how severe Sandy would have been if it had hit
244 the coastline during high tide. The hydrological distance (Table 1) of CI8 was only 2.9 km from the coastline,
245 making it the closest to the shore and the most susceptible to the altered scenario. Shifted tide increased the
246 inundation relative to the FEMA 100-year flood map for CI2 and CI4/5, suggesting shifted tide time alone can alter
247 the traditionally derived 100-year flood zone significantly.

248   The effects of compound events emerged drastically with the combination of shifted tide and SLR. Except for CI3
249   and CI8, all the CIs showed an increase in the percentage change from FEMA (Table 4). In comparison to SD1, SD3
250   showed increased inundation for all the CIs. The inundated area was about 146% more (1.9 km2) for SD3 than SD1
251   (0.9 km2) for CI1, for example. The flows for Sandy had a recurrence interval of about two years, but the flood
252   hazard associated with them became more devastating with the compound effect. For Florence and Irene, we saw an
253   increased flooded area in comparison to FEMA (Table 4); for CI2, for example, the increase was almost 200% from
254   IR1 to IR2. These results make it very clear that flow frequency cannot be the only measure to translate the severity
255   of a flood hazard.

256   For all the study sites for future Sandy, we saw consistent increases in flood extent (Table 4) from SD2 to SD4 and
257   SD3 to SD5. Between SD2/SD3 and SD4/SD5, the only difference was the future projection of the flow. In
258   comparison to the FEMA map, the percentage change ranged from –22.3 to +123.7. CI1, CI7, and CI8 for SD4 have
259   less inundation than the FEMA 100-year map. This may be an indication of the significance of individual flood
260   components specific to one site. For those sites, river flow might not be the most significant component of the flood.
261   When we look at the hydrologic distances in table 1 CI1 and CI8 are closer to the coastline, making them more
262   prone to coastal flooding than fluvial flooding. When we looked at SD5 (which added SLR), all the sites except CI8
263   showed more flooding than the FEMA 100-year flood map. Although CI8 had an increase of 22% in inundation
264   compared to SD4.

265   When we compare the worst-case future events (SD5 and IR2) to actual events (SD1 and IR1), we can see extreme
266   changes in flood extents. The flood extent in all locations increased by about 60% on average for future Sandy with
267   both SLR and coinciding tide (SD5) in comparison to the actual Sandy (SD1), with the highest impact in CI8
268   (+148%). Looking at Irene, the worst-case future scenario (IR2) increased the flood extent by about 30% on average
269   for all locations compared to the actual event (IR2), with the highest impact in CI2 (101%). Among all the events,
270   Florence had the lowest expected changes, between the current climate scenario (FL1) and the future one (FL2). One
271   must note that Florence had no actual impact in the study area; the simulation for this event was based on a possible
272   track forecast by GFS, showing it could have produced a flood inundation of almost 5 km2 in CI3, and that this
273   extent could have increased by about 20% in the worst-case future scenario (FL2) that included shifted tide and
274   SLR. Five of the CIs were exposed outside the FEMA 100-year flood zone for FL1 and SD3. For FL2 all of the
275   study sites were exposed to more vulnerability (positive % change) compared to FEMA map and for SD5, all the
276   sites except CI8.

277

278   **3.2 Flood depths over the domain**

279   To evaluate the flood hazard in terms of flood depth, we analysed the cumulative distribution function (CDF) of
280   maximum flood depths within the simulation domain. CDFs are effective for comparing flood damage among
281   different events (Hanman et al., 2016; Lin et al., 2016; Warner and Tissot 2012). From our analysis of the CDFs
282   (Figure 7) emerged the finding that the dependence among the combined effect of coastal water level, fluvial flow,
283   and tide strongly influenced the joint water depth probability and, in turn, implicated a higher vulnerability of the

284 CIs. For the same probability, the flood depth was greater for compound scenarios. This behaviour was consistent

285 for all CIs, as represented in Figure 7.

286 These results suggest that fluvial flow is not the only driver determining flood risk. Actual Irene (IR1) and synthetic

287 Florence (FL) had higher river flood return periods than did actual Sandy (SD1) (Table 2). Nonetheless, the CDFs of

288 the flood depth showed different behavior in terms of severity. For CI1, for example, IR1 had higher probabilities

289 for lower depth, followed by SD1 and FL1. In CI8, SD1 had higher probabilities for lower values of depth. These

290 findings highlight that neither the severity of rainfall nor the magnitude of river flows to control the flood extent and

291 flooded area characteristics, which are, rather, controlled by additional factors, such as storm surge, high tides,

292 topography, and location of the site. CI7, for example, which is more coastal than the other CIs, presented increasing

293 flood depth due to tidal timing.

294 As expected, and as previously highlighted when considering the flood extent (Table 4), climate played an important

295 role in flood hazard changes. Furthermore, the effect of SLR was also evident for all the events (IR, SD, and FL),

296 increasing the flood depth for the same exceedance probability. For CI6, for example, the 50% exceedance

297 corresponded to ~1 m depth of floodwater for IR1, increasing to ~1.5 m for IR2. For the CI4 and CI5 sites, for

298 exceedance of 20%, actual Irene produced ~2 m of flood depth, whereas with SLR it was ~2.5 m. Another way to

299 put it is that, for CI4/5, IR1 had an exceedance of ~20% for a flood depth of 2 m, whereas IR2 had an increased

300 exceedance level of 40%. Similarly, for 50% exceedance, FL1 and FL2 corresponded to 1.5 m and 2 m depth of

301 floodwater, respectively, and we also saw the trend for the Sandy event scenarios (SD2–SD3; SD4–SD5). In short,

302 this trend could be seen for almost all the sites and is an indication of how a projected increase of SLR due to

303 climate change might affect the risk of flood hazard at a location.

304 This analysis highlighted that the timing of a storm is also crucial. The changes from SD1 to SD2 showed very well

305 the impact of the shifted tide for all the sites. For CI3, for example, the 1 m flood depth had an exceedance of ~88%

306 for SD2, whereas it was only ~23% for SD1.

307 These findings show that the coincidence of high tide and storm surge results in a significant increase in flood risk.

308 SD3 and SD5 had all the components of a compound flood and comparing them with SD1 gave us a clear idea of

309 how severe a compound event can be in the future. CI3, for example, had exceedance levels of almost 30%, 85%,

310 and 90%, respectively, for SD1, SD3, and SD5 for a flood depth of 1 m. This suggests the compound effect

311 increases the intensity of the flood hazard.

312 **3.3 Local risk for CI**

313 Figure 8 shows for each CI the percentage of the time that selected water level thresholds were exceeded. CI1 was

314 never flooded for any of the scenarios. For the other CIs, in comparisons of individual events we could see an

315 increase in risk due to the added compound hazard scenarios—that is, shifted tide and SLR. Important to note is that,

316 for most of the sites, the compound risk due to SLR and tide timing was always higher for the lower water-level

317 thresholds (0.5 m). This implies a higher risk for CI components currently positioned closer to the ground. Much of

318 the flood damage in CI is incurred by components being underwater for a longer time. The results of the analysis

319 (Figure 8) should be considered in planning for any protective measures, such as elevating or waterproofing

320 equipment. The suggested high values of risk [increase percentage in time-specific depths are maintained] (Figure 8)

321 also imply differences in the timing of repairs. Therefore, damage to the CI components is dictated by both the flood

322 depth and the duration of submergence. In the cases of CI7 and CI8 (Figure 8), the CIs remained submerged in 0.5

323 m of water for about 20% of the event period for actual Sandy, but for the worst-case future Sandy scenario, we

324 found the time of submergence increased to 90% of the event period. This demonstrates the increased flood risk to

325 which future climate conditions expose CI.

326 Another important insight was provided by the hurricane Florence scenarios. As mentioned earlier, Florence did not

327 affect the study area, although an early GFS storm forecast track predicted landfall in Long Island and Connecticut.

328 For this event, the estimated measure of risk was about 20%, and it was shown to increase to up to 40% for the

329 lower water depth (0.5 m) threshold in some locations. The result of the simulated scenario allows for an assessment

330 of potential damage and for an identification of equipment that might be affected by future events under current

331 climatic conditions. In this regard, comparing the results for the different CIs during the Sandy scenarios revealed an

332 interesting pattern. While we might have expected a greater impact over the whole domain when shifting the tide

333 (Figure 8, Table. 3), we found instead different impacts in the different CI locations. Notably, the risk appeared

334 lower when the tides were shifted (Fig. 8) for some of the CIs (for example, CI5 and CI7). This can be explained by

335 the fact that higher water levels in the domain were changing the water flows, allowing the flood to follow different

336 drainable ways. This can be a very useful piece of information for deciding whether to and where to take measures

337 in terms of flood occurrence and potentially relocating CIs to avoid catastrophic compound flood events.

338 Generally, hurricanes affect large areas, and the specific locations at which damage will occur are often difficult to

339 anticipate. Simulation of different scenarios can provide system operators with the ability to prepare for damage and

340 respond quickly once it has occurred—for example, by pre-positioning repair crews. From table 1 we can see that

341 CI8 is the closest to the coastline followed by CI7, CI6, and CI5. From figure 8 we can see that all the CIs that are

342 closer to the coastline are susceptible to changes in the downstream water level condition (Shifted tide/ SLR) (Table

343 4). CI4 is the farthest from the coast followed by CI3. Both the CIs show minimal response to changes in the coastal

344 water level compared to CI5/ CI6/ CI7. This analysis gives us conclusive evidence of risk associated with the

345 location of the CI from the coastline.

346 **4 Concluding Remarks**

347 This study evaluated the compound effect of different flood drivers (rainfall, surge, SLR, tides) for critical

348 infrastructure in coastal areas, based on case studies of actual and synthetic hurricane events in the north-eastern

349 United States. The proposed framework offers an approach to estimate the potential impacts of extreme compound

350 hazards, which is vital for developing mitigation strategies. The framework will allow researchers and stakeholders

351 to analyse the effects of combined hazards and prepare to take necessary measures to protect the vulnerable

352 infrastructure within the flood zone.

353 The findings of this study can support flood mitigation; the FEMA 100-year map is used for designing infrastructure

354 and for making decisions on flood mitigation and flood insurance. Our results, however, show this map does not

355 account for the impacts posed by simultaneous conditions, such as high tide and river flows, or for future climate

356 impacts. They show how the vulnerability of each substation is linked to the different storms, and how this varies

357 depending on the distance from the coast—that is, inland substations are less affected by surge and SLR and more

358 affected by rainfall accumulation events (such as Irene). The findings of this study highlight that rising seas will

359 allow storm surges to inundate areas farther inland and that flood hazard is likely to grow as seas rise and storm

360 surges become deeper.

361 Future research should consider improved estimation methods, including more detailed river properties (such as

362 channel depth and width), and should relate the frequency of hurricanes and tropical cyclones to return periods of

363 precipitation, river flows, and surges, as well as differentiate among the individual effects of the components to

364 determine the role of each in flooding impact. This can be a very useful piece of information for deciding whether

365 and where to take measures in terms of flood occurrence and the potential relocation of CI to avoid catastrophic

366 compound flood events.

367 Notwithstanding these challenges, the findings of this study highlight that, whenever possible, risk assessments

368 across different critical locations directly or indirectly affecting critical infrastructure should be based on a

369 consistent set of compound risks. Critical infrastructure is usually positioned by following the FEMA 100-year flood

370 zone map. The areas outside the map are without mitigation plans and stand without any protection, on the other

371 hand, these plans are based on some certain flood depth. In this study, however, we see an increase in flooded areas

372 in the futuristic scenarios, as well as some under- and overestimation from the FEMA map, and that the flood depth

373 at a location can essentially increase during a compound flooding. This may bring us to the conclusion that

374 compound flooding extends the areas to be included in mitigation plans.

375 The proposed analysis suggests planning and management strategies for critical infrastructure should rely on

376 historical flooding data, together with future storm scenarios and climate and SLR projections. This will ultimately

377 allow the building of resilience into different components of critical infrastructure to enable the system to function

378 even under disaster conditions or to recover more quickly.

379

380 **Acknowledgements**: This work was supported by Eversource Energy.

381 **Author contributions:** MKh, GS, XS, EA conceived the study. XS and EA contributed to the conception of the

382 hydrologic model. RL contributed to the production and analysis of the hydrologic model outputs. MKo and EN

383 contributed to the analysis, and interpretation of the climatic data. MKh and GS contributed to the automation of the

384 hydraulic model and interpretation of its results. All authors participated in drafting the article and revising it

385 critically for important intellectual content. All authors give final approval of the published version.

386 **Competing interests.** The authors declare that they have no conflict of interest.
387

388 **References**

389 Barnard, P. L., Erikson, L. H., Foxgrover, A. C., Hart, J. A. F., Limber, P., O'Neill, A. C., … Jones, J. M.: Dynamic
390 flood modeling essential to assess the coastal impacts of climate change. Scientific Reports, 9(1), 4309.
391 https://doi.org/10.1038/s41598-019-40742-z, 2019.

392 Bevacqua, E., Maraun, D., Vousdoukas, M. I., Voukouvalas, E., Vrac, M., Mentaschi, L., Widmann, M.: Higher
393 probability of compound flooding from precipitation and storm surgein Europe under anthropogenic climate change.
394 Sci. Adv. 5, eaaw5531, 2019.

395 Blöschl, G., Hall, J., Parajka, J., Perdigão, R. A. P., Merz, B., Arheimer, B., Aronica, G. T., Bilibashi, A., Bonacci,
396 O., Borga, M., Čanjevac, I., Castellarin, A., Chirico, G. B., Claps, P., Fiala, K., Frolova, N., Gorbachova, L., Gül,
397 A., Hannaford, J., Harrigan, S., Kireeva, M., Kiss, A., Kjeldsen, T. R., Kohnová, S., Koskela, J. J., Ledvinka, O.,
398 Macdonald, N., Mavrova-Guirguinova, M., Mediero, L., Merz, R., Molnar, P., Montanari, A., Murphy, C., Osuch,
399 M., Ovcharuk, V., Radevski, I., Rogger, M., Salinas, J. L., Sauquet, E., Šraj, M., Szolgay, J., Viglione, A., Volpi, E.,
400 Wilson, D., Zaimi, K. and Živković, N.: Changing climate shifts timing of European floods, Science (80-.).,
401 357(6351), 588–590, doi:10.1126/science.aan2506, 2017.

402 Bunya, S., Dietrich, J. C., Westerink, J. J., Ebersole, B. A., Smith, J. M., Atkinson, J. H., … Roberts, H. J.: A High-
403 Resolution Coupled Riverine Flow, Tide, Wind, Wind Wave, and Storm Surge Model for Southern Louisiana and
404 Mississippi. Part I: Model Development and Validation. Monthly Weather Review, 138(2), 345–377.
405 https://doi.org/10.1175/2009MWR2906.1, 2010.

406 Cañizares, R., & Irish, J. L.: Simulation of storm-induced barrier island morphodynamics and flooding. Coastal
407 Engineering, 55(12), 1089–1101. https://doi.org/10.1016/J.COASTALENG.2008.04.006, 2008.

408 Cariolet, J.-M.: Use of high water marks and eyewitness accounts to delineate flooded coastal areas: The case of
409 Storm Johanna (10 March 2008) in Brittany, France. Ocean & Coastal Management, 53(11), 679–690.
410 https://doi.org/10.1016/J.OCECOAMAN.2010.09.002, 2010.

411 Chang, S. E., McDaniels, T. L., Mikawoz, J., Peterson, K.: Infrastructure failure interdependencies in extreme
412 events: power outage consequences in the 1998 Ice Storm. Nat Hazards 41:337–358. doi: 10.1007/s11069-006-
413 9039-4, 2007.

414 Chang, S. E., McDaniels, T. L., Mikawoz, J., & Peterson, K.: Infrastructure failure interdependencies in extreme
415 events: power outage consequences in the 1998 Ice Storm. Natural Hazards, 41(2), 337–358.
416 https://doi.org/10.1007/s11069-006-9039-4, 2007.

417 Chou M.-D., and Suarez, M. J.: An efficient thermal infrared radiation parameterization for use in general
418 circulation models. NASA Tech. Memo. 104606, 3, 85pp, 1994.

419 CtECO, C. E. C. O.: Connecticut Elevation (Lidar) Data, 2016.

420 Danielson, J.J. and Gesch, D.B.: Global multi-resolution terrain elevation data 2010 (GMTED2010) (p. 26). US
421 Department of the Interior, US Geological Survey, 2016.

422 Dawson, R. J., Thompson, D., Johns, D., Wood, R., Darch, G., Chapman, L., Hughes, P. N., Watson, G. V. R.,
423 Paulson, K., Bell, S., Gosling, S. N., Powrie, W. and Hall, J. W.: A systems framework for national assessment of

climate risks to infrastructure, Philos. Trans. R. Soc. A Math. Phys. Eng. Sci., 376(2121), doi:10.1098/rsta.2017.0298, 2018.

de Bruijn, K., Buurman, J., Mens, M., Dahm, R. and Klijn, F.: Resilience in practice: Five principles to enable societies to cope with extreme weather events, Environ. Sci. Policy, 70, 21–30, doi:10.1016/j.envsci.2017.02.001, 2017.

de Bruijn, K. M., Maran, C., Zygnerski, M., Jurado, J., Burzel, A., Jeuken, C. and Obeysekera, J.: Flood resilience of critical infrastructure: Approach and method applied to Fort Lauderdale, Florida, Water (Switzerland), 11(3), doi:10.3390/w11030517, 2019.

Dottori, F., Szewczyk, W., Ciscar, J. C., Zhao, F., Alfieri, L., Hirabayashi, Y., Bianchi, A., Mongelli, I., Frieler, K., Betts, R. A. and Feyen, L.: Increased human and economic losses from river flooding with anthropogenic warming, Nat. Clim. Chang., 8(9), 781–786, doi:10.1038/s41558-018-0257-z, 2018.

FAO.: The digitized soil map of the world, World Soil Resource Rep. 67, FAO, Rome. FAO-UNESCO (1971–1981), Soil Map of the World (1:5,000,000), vol. 1–10, UNESCO, Paris, France. FAO-UNESCO (1974), Soil Map of the World (1:5,000,000), vol. 1 legend, UNESCO, Paris, France, 1991.

FEMA.: Reducing Flood Effects in Critical Facilities. HSFE60-13-(April), 1–11, 2013.

Friedl, M., Sulla-Menashe, D.: MCD12Q1 MODIS/Terra+Aqua Land Cover Type Yearly L3 Global 500m SIN Grid V006. NASA EOSDIS Land Processes DAAC. https://doi.org/10.5067/MODIS/MCD12Q1.006, 2015.

Friedl M. A., Sulla-Menashe D., Tan B., Schneider A., Ramankutty N., Sibley A., & Huang X.: MODIS Collection 5 global land cover: Algorithm refinements and characterization of new datasets. Remote Sensing of Environment, 114(1), 168 10.1016/j.rse.2009.08.016–182), 2010.

Gerald, A. M., Covey, C, Delworth, T., Latif, M., McAvaney, B., Mitchell, J. F. B., Stouffer, R. J., and Taylor, K. E.: The WCRP CMIP3 multimodel dataset: A new era in climate change research. Bulletin of American Meteorological Society, 2007.

Grell, G. A., and Dévényi, D., A generalized approach to parameterizing convection combining ensemble and data assimilation techniques, Geophys. Res. Lett., 29(14), doi:10.1029/2002GL015311, 2002.

Hallegatte, S., Green, C., Nicholls, R. J., Corfee-Morlot, J.: Future flood losses in major coastal cities. Nat Clim Chang 3:802–806. doi: 10.1038/nclimate1979, 2013.

Hamman, J. J., Hamlet, A. F., Lee, S.-Y., Fuller, R., & Grossman, E. E.: Combined Effects of Projected Sea Level Rise, Storm Surge, and Peak River Flows on Water Levels in the Skagit Floodplain. Northwest Science, 90(1), 57–78. https://doi.org/10.3955/046.090.0106, 2016.

Hardesty, S., Shen, X., Nikolopoulos, E., & Anagnostou, E.: A Numerical Framework for Evaluating Flood Inundation Hazard under Different Dam Operation Scenarios—A Case Study in Naugatuck River. Water, 10(12), 1798. https://doi.org/10.3390/w10121798, 2018.

Higgins, R.W.: Climate Prediction Center (U.S.). Improved United States Precipitation Quality Control System and Analysis; NCEP/Climate Prediction Center Atlas, NOAA, National Weather Service, National Centers for Environmental Prediction, Climate Prediction Center: Camp Springs, MD, USA, 2000.

460 Hostache, R., Matgen, P., Schumann, G., Puech, C., Hoffmann, L., & Pfister, L.: Water Level Estimation and
461 Reduction of Hydraulic Model Calibration Uncertainties Using Satellite SAR Images of Floods. IEEE Transactions
462 on Geoscience and Remote Sensing, 47(2), 431–441. https://doi.org/10.1109/TGRS.2008.2008718, 2009.

463 Karagiannis, G.M., Chondrogiannis, S., Krausmann, E. and Turksezer, Z.I.: Power grid recovery after natural
464 hazard impact. Science for Policy report by the Joint Research Centre   (JRC),   European   Union.
465 https://doi.org/10.2760/87402, 2017.

466 Koenig, T.A., Bruce, J.L., O'Connor, J.E., McGee, B.D., Holmes, R.R., Jr., Hollins, Ryan, Forbes, B.T., Kohn,
467 M.S., Schellekens, M.F., Martin, Z.W., and Peppler, M.C.: Identifying and preserving high-water mark data: U.S.
468 Geological Survey Techniques and Methods,   book 3, chap. A24, 47 p., http://dx.doi.org/10.3133/tm3A24,
469 2016.

470 Lackmann, G. M.: Hurricane Sandy before 1900, and after 2100. Bull. Amer. 699 Meteor. Soc., 96, 547-560, doi:
471 10.1175/BAMS-D-14-00123.1, 2015.

472 Leonard, M., Westra, S., Phatak, A., Lambert, M., Van Den Hurk, B., Mcinnes, K., … Stafford-Smith, M.: A
473 compound event framework for understanding extreme impacts. WIREs Clim Change, 5, 113–128.
474 https://doi.org/10.1002/wcc.252, 2014.

475 Lin, N., Kopp, R. E., Horton, B. P., & Donnelly, J. P.: Hurricane Sandy's flood frequency increasing from year 1800
476 to 2100. Proceedings of the National Academy of Sciences of the United States of America, 113(43), 12071–12075.
477 https://doi.org/10.1073/pnas.1604386113, 2016.

478 Marsooli, R., Lin, N., Emanuel, K., & Feng, K.: Climate change exacerbates hurricane flood hazards along US
479 Atlantic and Gulf Coasts in spatially varying patterns. Nature Communications,   10(1).
480 https://doi.org/10.1038/s41467-019-11755-z, 2019.

481 McEvoy, D., Ahmed, I., Mullett, J.: The impact of the 2009 heat wave on Melbourne's critical infrastructure. Local
482 Environ 17:783–796. doi: 10.1080/13549839.2012.678320, 2012.

483 Mlawer, E. J., Taubman, S. J., Brown, P. D., Iacono, M. J. and Clough, S. A.: Radiative transfer for inhomogeneous
484 atmospheres: RRTM, a validated correlated–k model for the longwave. J. Geophys. Res., 102, 16663–16682.
485 doi:10.1029/97JD00237, 1997.

486 Moftakhari, H. R., Salvadori, G., AghaKouchak, A., Sanders, B. F., & Matthew, R. A.: Compounding effects of sea
487 level rise and fluvial flooding. Proceedings of the National Academy of Sciences of the United States of America,
488 114(37), 9785–9790. https://doi.org/10.1073/pnas.1620325114, 2017.

489 Muis, S., Verlaan, M., Winsemius, H. C., Aerts, J. C. J. H. and Ward, P. J.: A global reanalysis of storm surges and
490 extreme sea levels, Nat. Commun., 7, doi:10.1038/ncomms11969, 2016.

491 NOAA.: NOAA's STATE OF THE COAST: National Coastal Population Report, 2013.

492 O'Donnell, J.: Sea Level Rise Connecticut Final Report. https://circa.uconn.edu/wp-
493 content/uploads/sites/1618/2019/02/SeaLevelRiseConnecticut-Final-Report.pdf, 2017. (last accessed January 10,
494 2020)

495 Pant, R., Thacker, S., Hall, J. W., Alderson, D. and Barr, S.: Critical infrastructure impact assessment due to flood
496 exposure, J. Flood Risk Manag., 11(1), 22–33, doi:10.1111/jfr3.12288, 2018.

497   Pearson, J., Punzo, G., Mayfield, M., Brighty, G., Parsons, A., Collins, P., Jeavons, S. and Tagg, A.: Flood

498   resilience: consolidating knowledge between and within critical infrastructure sectors, Environ. Syst. Decis., 38(3),

499   318–329, doi:10.1007/s10669-018-9709-2, 2018.

500   Powers, J. G., Klemp, J. B., Skamarock, W. C., Davis, C. A., Dudhia, J., Gill, D. O., Coen, J. L. and Gochis, D. J.:

501   The Weather Research and Forecasting Model: Overview,   system efforts, and future directions. Bull. Amer.

502   Meteor. Soc., 98, 1717   1737, https://doi.org/10.1175/BAMS-D-15-00308.1, 2017.

503   Quinn, N., Bates, P. D., Neal, J., Smith, A., Wing, O., Sampson, C., Smith, J. and Heffernan, J.: The Spatial

504   Dependence of Flood Hazard and Risk in the United States, Water Resour. Res., 55(3), 1890–1911,

505   doi:10.1029/2018WR024205, 2019.

506   Schumann, G., Hostache, R., Puech, C., Hoffmann, L., Matgen, P., Pappenberger, F., & Pfister, L.: High-Resolution

507   3-D Flood Information From Radar Imagery for Flood Hazard Management. IEEE Transactions on Geoscience and

508   Remote Sensing, 45(6), 1715–1725. https://doi.org/10.1109/TGRS.2006.888103, 2007.

509   Schumann, G., Matgen, P., Cutler, M. E. J., Black, A., Hoffmann, L., & Pfister, L.: Comparison of remotely sensed

510   water stages from LiDAR, topographic contours and SRTM. ISPRS Journal of Photogrammetry and Remote

511   Sensing, 63(3), 283–296. https://doi.org/10.1016/J.ISPRSJPRS.2007.09.004, 2008.

512   Schumann, G., Matgen, P., Hoffmann, L., Hostache, R., Pappenberger, F., & Pfister, L.: Deriving distributed

513   roughness values from satellite radar data for flood inundation modelling. Journal of Hydrology, 344(1–2), 96–111.

514   https://doi.org/10.1016/J.JHYDROL.2007.06.024, 2007.

515   Shen, X., & Anagnostou, E. N.: A framework to improve hyper-resolution hydrological simulation in snow-affected

516   regions. Journal of Hydrology, 552, 1–12. https://doi.org/10.1016/j.jhydrol.2017.05.048, 2017.

517   Skamarock, W. C., Klemp, J. B., Dudhia, J., Gill, D. O., Barker, D. M., Duda, M. G., Huang, X., Wang, W. and

518   Powers, J. G.: A description of the Advanced Research WRF version   3. NCAR Tech. Note NCAR/TN-475+STR,

519   113   pp., https://doi .org/10.5065/D68S4MVH, 2008.

520   Song–You, H., Noh, Y. and Dudhia, J.: A new vertical diffusion package with an   explicit   treatment   of

521   entrainment processes. Mon. Wea. Rev., 134, 2318   2341. doi:10.1175/MWR3199.1, 2006.

522   Tewari, M.F., Chen, W., Wang, J., Dudhia, M.A., LeMone, K., Mitchell, M.E., Gayno, G., Wegiel, J. and Cuenca,

523   R.H.: Implementation and verification of the unified NOAH   land surface model in the WRF model. 20th

524   conference on weather analysis and forecasting/16th conference on numerical weather prediction, pp. 11–15, 2004.

525   Thompson, G., Paul, R. F., Roy, M. R. & William, D. H.: Explicit Forecasts   of Winter Precipitation Using an

526   Improved Bulk Microphysics Scheme. Part II: Implementation of a New Snow Parameterization. Mon. Wea.

527   Rev., 136, 5095–5115.   doi:10.1175/2008MWR2387.1, 2008.

528   U.S. Geological Survey.: 1/9th Arc-second Digital Elevation Models (DEMs) - USGS National Map 3DEP

529   Downloadable Data Collection: U.S. Geological Survey., 2017.

530   Vousdoukas, M. I., Mentaschi, L., Voukouvalas, E., Verlaan, M., Jevrejeva, S., Jackson, L. P. and Feyen, L.: Global

531   probabilistic projections of extreme sea levels show intensification of coastal flood hazard, Nat. Commun., 9(1), 1–

532   12, doi:10.1038/s41467-018-04692-w, 2018.

533   Wahl, T., Jain, S., Bender, J., Meyers, S. D., & Luther, M. E.: Increasing risk of compound flooding from storm
534   surge and rainfall for major US cities. Nature Climate Change, 5(12), 1093–1097.
535   https://doi.org/10.1038/nclimate2736, 2015.

536   Wahl, T., Ward, P., Winsemius, H., AghaKouchak, A., Bender, J., Haigh, I., … Westra, S.: When Environmental
537   Forces Collide. Eos, 99. https://doi.org/10.1029/2018EO099745, 2018.

538   Warner, N. N., & Tissot, P. E.: Storm flooding sensitivity to sea level rise for Galveston Bay, Texas. Ocean
539   Engineering, 44, 23–32. https://doi.org/10.1016/J.OCEANENG.2012.01.011, 2012.

540   Vousdoukas, M. I., Mentaschi, L., Voukouvalas, E., Verlaan, M., Jevrejeva, S., Jackson, L. P. and Feyen, L.: Global
541   probabilistic projections of extreme sea levels show intensification of coastal flood hazard, Nat. Commun., 9(1), 1–
542   12, doi:10.1038/s41467-018-04692-w, 2018.

543   Winsemius, H. C., Van Beek, L. P. H., Jongman, B., Ward, P. J. and Bouwman, A.: A framework for global river
544   flood risk assessments, Hydrol. Earth Syst. Sci, 17, 1871–1892, doi:10.5194/hess-17-1871-2013, 2013.

545   Xia, Y., Mitchell, K., Ek, M., Sheffield, J., Cosgrove, B., Wood, E., … Mocko, D. .: Continental-scale water and
546   energy flux analysis and validation for the North American Land Data Assimilation System project phase 2
547   (NLDAS-2): 1. Intercomparison and application of model products. Journal of Geophysical Research: Atmospheres,
548   117(D3), n/a-n/a. https://doi.org/10.1029/2011JD016048, 2012.

549   Ziervogel, G., New, M., Archer van Garderen, E., Midgley, G., Taylor, A., Hamann, R., Stuart-Hill, S., Myers, J.
550   and Warburton, M.: Climate change impacts and adaptation in South Africa. Wiley Interdiscip Rev Clim Chang
551   5:605–620. doi: 10.1002/wcc.295, 2014.

552   Ziervogel, G., New, M., Archer van Garderen, E., Midgley, G., Taylor, A., Hamann, R., … Warburton, M.: Climate
553   change impacts and adaptation in South Africa. Wiley Interdisciplinary Reviews: Climate Change, 5(5), 605–620.
554   https://doi.org/10.1002/wcc.295, 2014.

555   Zscheischler, J., Westra, S., van den Hurk, B. J. J. M., Seneviratne, S. I., Ward, P. J., Pitman, A., … Zhang, X.:
556   Future climate risk from compound events. Nature Climate Change, 8(6), 469–477. https://doi.org/10.1038/s41558-
557   018-0156-3, 2018.

558   Dee, D.P., Uppala, S.M., Simmons, A.J., Berrisford, P., Poli, P., Kobayashi, S., Andrae, U., Balmaseda, M.A.,
559   Balsamo, G., Bauer, P., Bechtold, P., Beljaars, A.C.M., van de Berg, L., Bidlot, J., Bormann, N., Delsol, C.,
560   Dragani, R., Fuentes, M., Geer, A.J., Haimberger, L., Healy, S.B., Hersbach, H., Hólm, E.V., Isaksen, L., Kållberg,
561   P., Köhler, M., Matricardi, M., McNally, A.P., Monge-Sanz, B.M., Morcrette, J.-J., Park, B.-K., Peubey, C., de
562   Rosnay, P., Tavolato, C., Thépaut, J.-N. and Vitart, F.: The ERA-Interim reanalysis: Configuration and performance
563   of the data assimilation system. Quart. J. Roy. Meteor. Soc., 137, 553–597, doi: https://doi.org/10.1002/qj.828,
564   2011.

565   Meehl, G. A., C. Covey, K. E. Taylor, T. Delworth, R. J. Stouffer, M. Latif, B. McAvaney, and J. F. B. Mitchell:
566   The WCRP CMIP3 multimodel dataset: A new era in climate change research. Bull. Amer. Meteor, 2007.

567

568

569
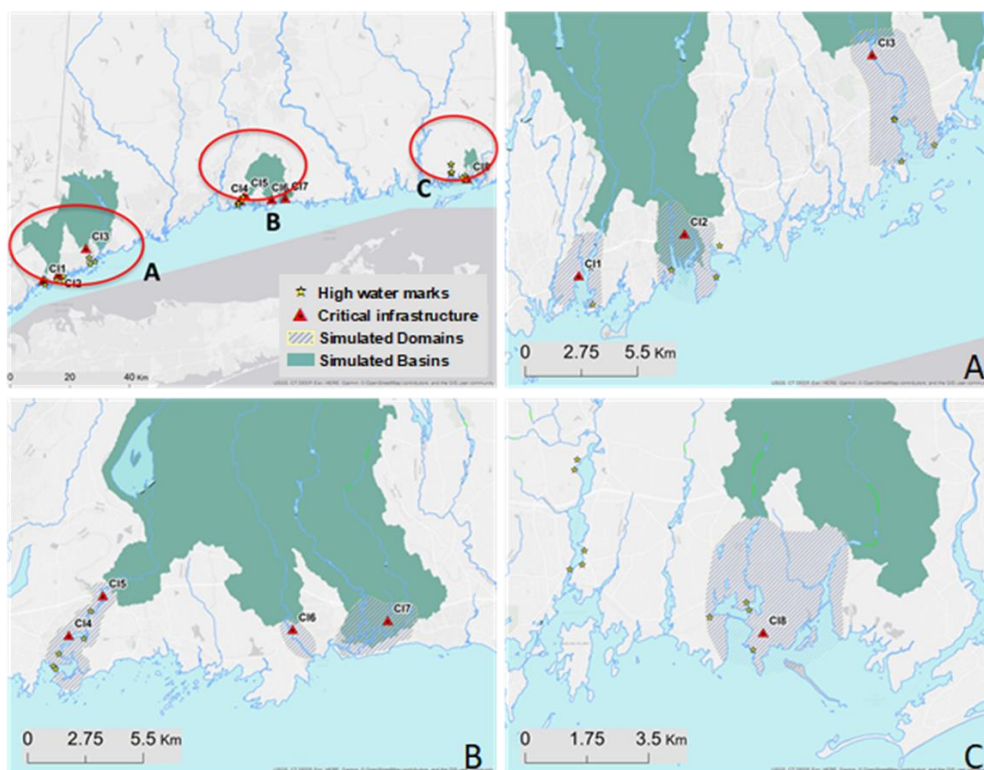
Figure 1: Study area with associated watersheds and simulation domains. Locations of substations and USGS high water marks is also shown. Red circles in the top left-hand panel, and marked with A, B and C are highlighted in the panels A to C respectively. Background map by ESRI web-services, provided by UConn/CTDEEP, Esri, Garmin, USGS, NGA, EPA, USDA, NPS
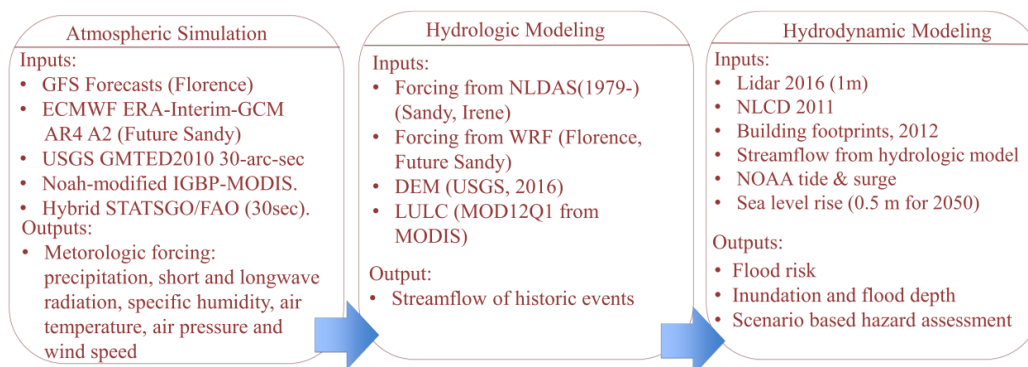
Figure 2: Considered framework including atmospheric simulations, hydrologic and hydrodynamic modeling. Hurricane events (actual and simulated), and inputs and outputs of each component are shown. Readers should refer to chapter 2.2 for specifications
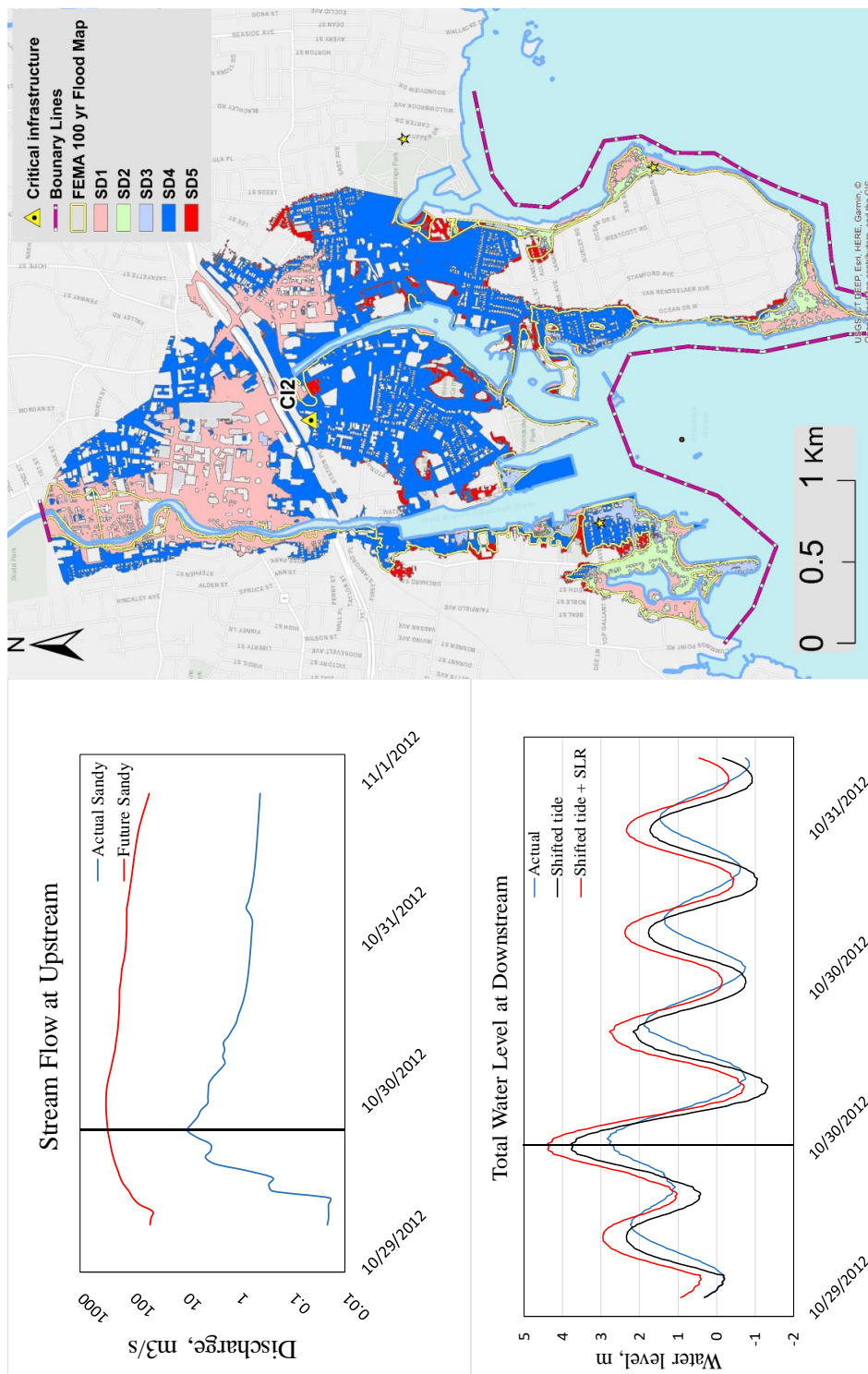
Figure 3: Example of different scenarios showing the upstream boundary condition (top left-hand panel, including the discharge for actual Sandy and future Sandy), and downstream boundary (bottom left-hand panel, including tide, shifted tide, and shifted tide with SLR). Output flood extend is also shown (right-hand panel, including results for SD1 to SD5 [reader should refer to Tab. 3 and chapter 2.2 for specification on the scenarios]). Background map on the firhtg-hand panel by ESRI web-services, provided by UConn/CTDEEP, Esri, Garmin, USGS, NGA, EPA, USDA, NPS
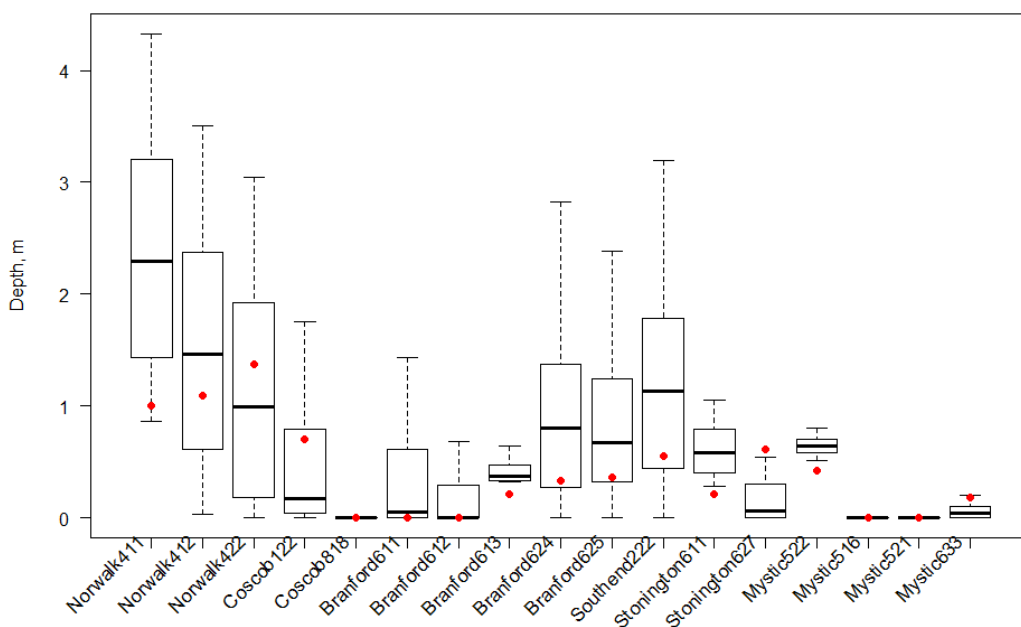
Figure 4: Validation results (boxplot of water depth within 10x10m around the high-water mark -HWM- location) compared to selected HWM (red dots) by USGS
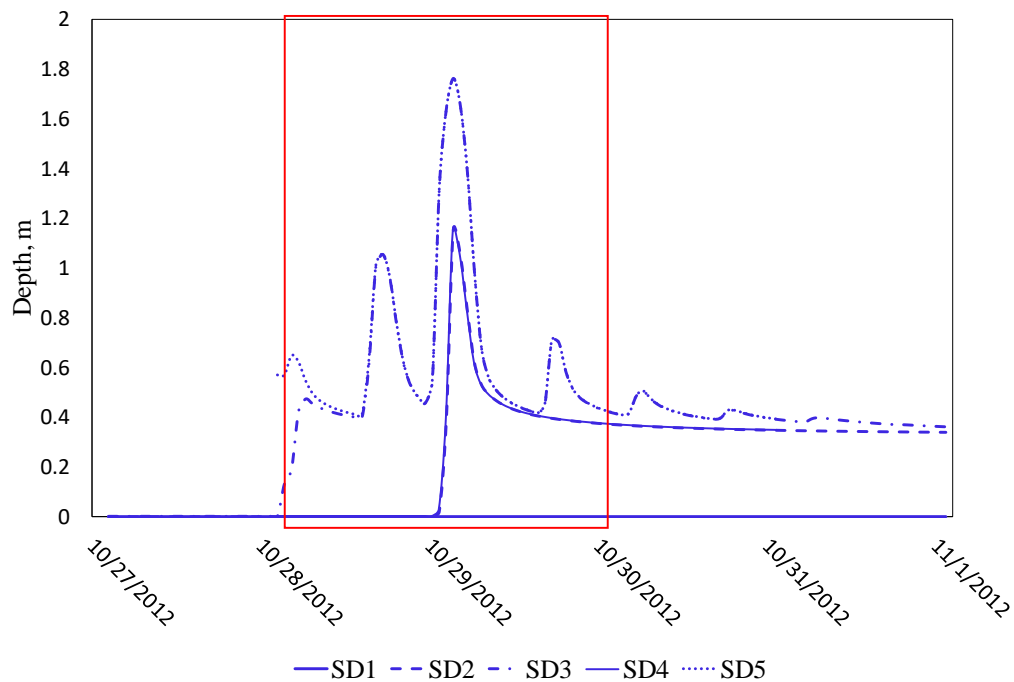
Figure 5: Example of time series of depth values for the different scenarios of Sandy event [SD1 to SD5, readers should refer to Table 3 and chapter 2.2 for specification on the scenarios] (Red rectangle shows the considered 24 hours window around the peak flow for calculation of the peak over threshold)
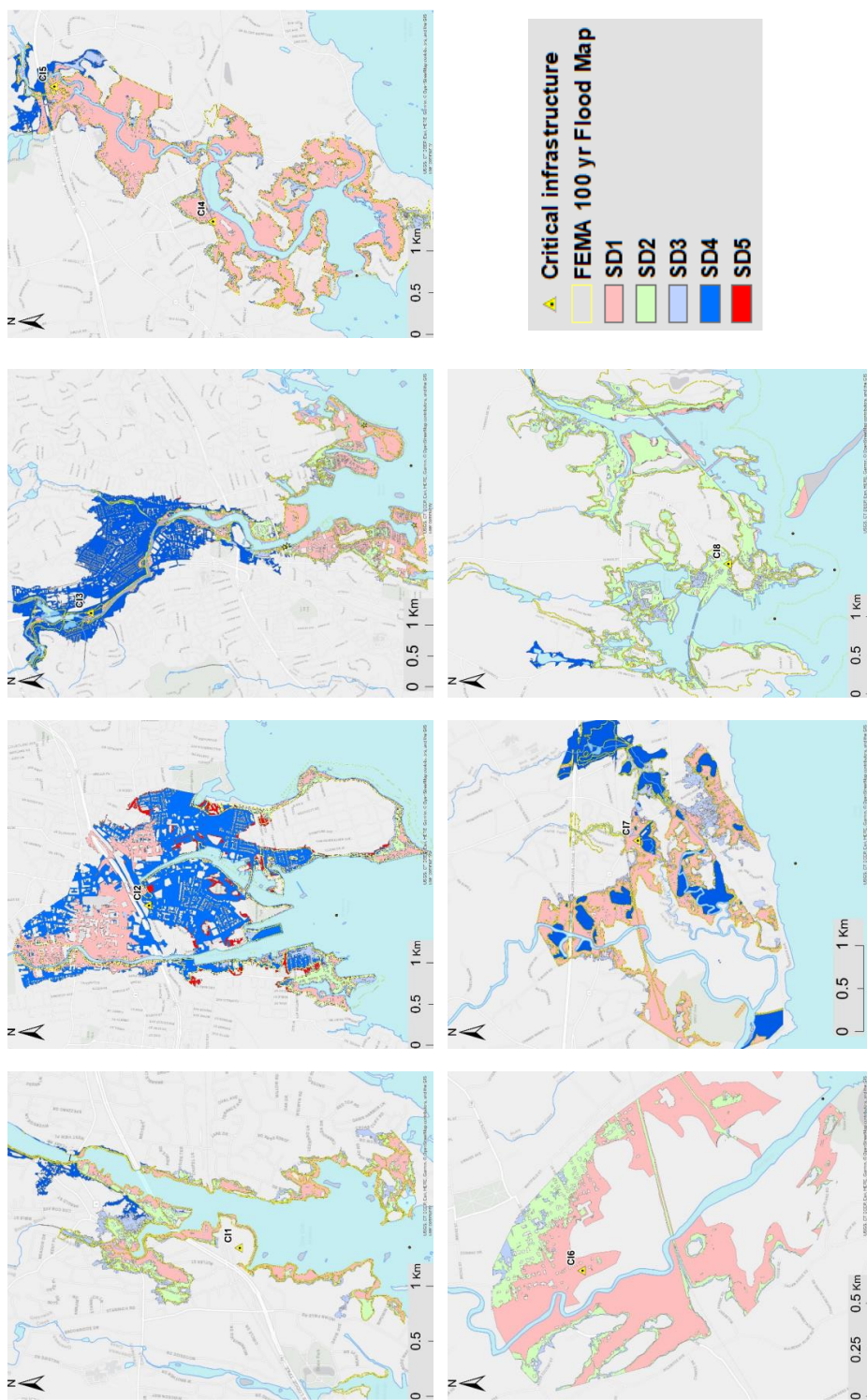
Figure 6a: Map overlay of maximum inundation for all the study domains containing CI1 through CI8 for the scenarios of Sandy [SD1 to SD5, readers should refer to Table 3 and chapter 2.2 for specification on the scenarios]
Figure 6b: Map overlay of maximum inundation for all the study domains containing CI1 through CI8 for the scenarios of Irene [IR1 and IR2, readers should refer to Tab. 3 and chapter 2.2 for specification on the scenarios]. Background map by ESRI web-services, provided by UConn/CTDEEP, Esri, Garmin, USGS, NGA, EPA, USDA, NPS
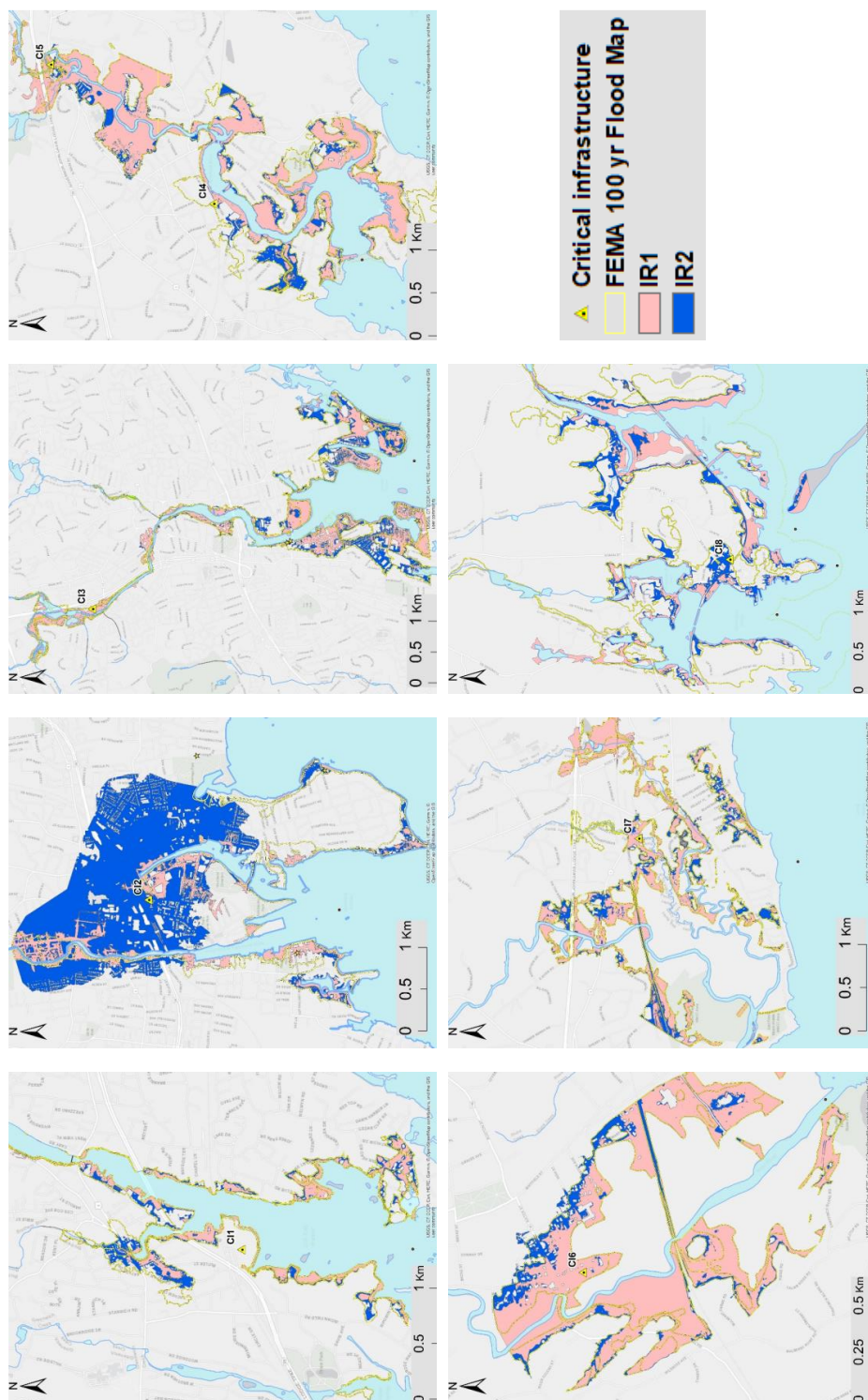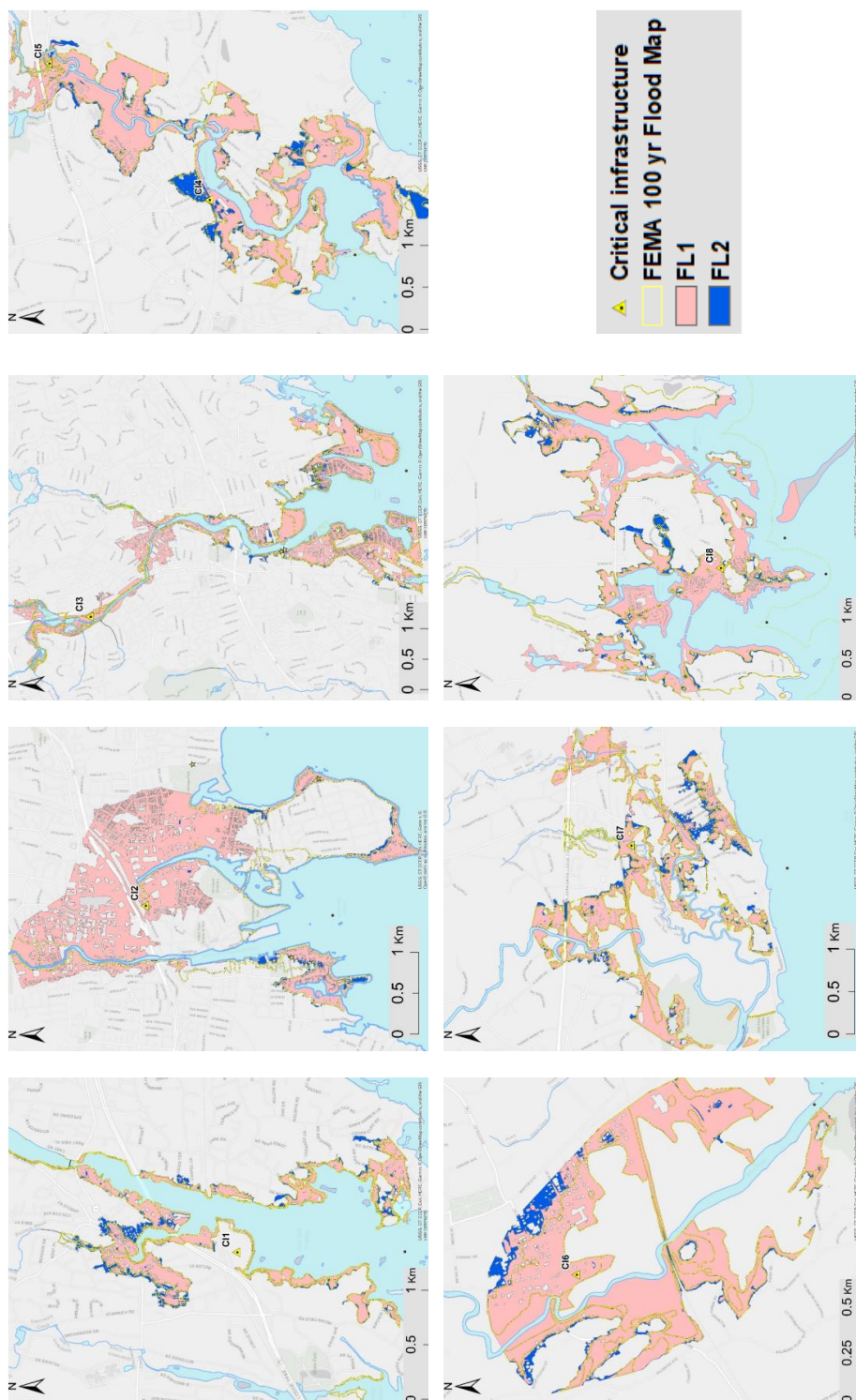
Figure 6c: Map overlay of maximum inundation for all the study domains containing CI1 through CI8 for the scenarios of Florence [FL1 and FL2, readers should refer to Table 3 and chapter 2.2 for specification on the scenarios]. Background map by ESRI web-services, provided by UConn/CTDEEP, Esri, Garmin, USGS, NGA, EPA, USDA, NPS
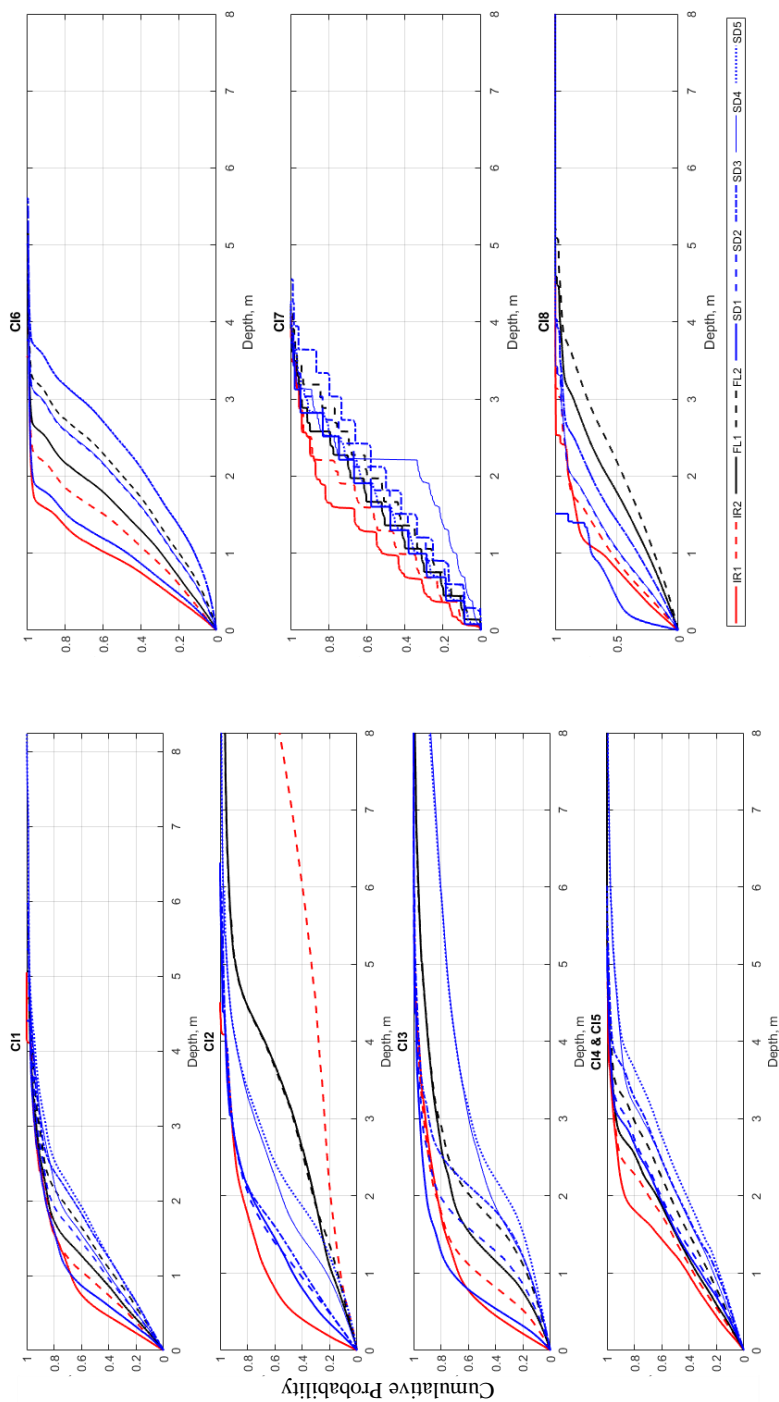
Figure 7: Cumulative density plot of the depth of all the flooded cells during maximum inundation. Hurricanes scenarios are labelled according to Table 3 and explained in chapter 2.2. Critical infrastructures are labelled CI1 to CI8, as described in Table 1.
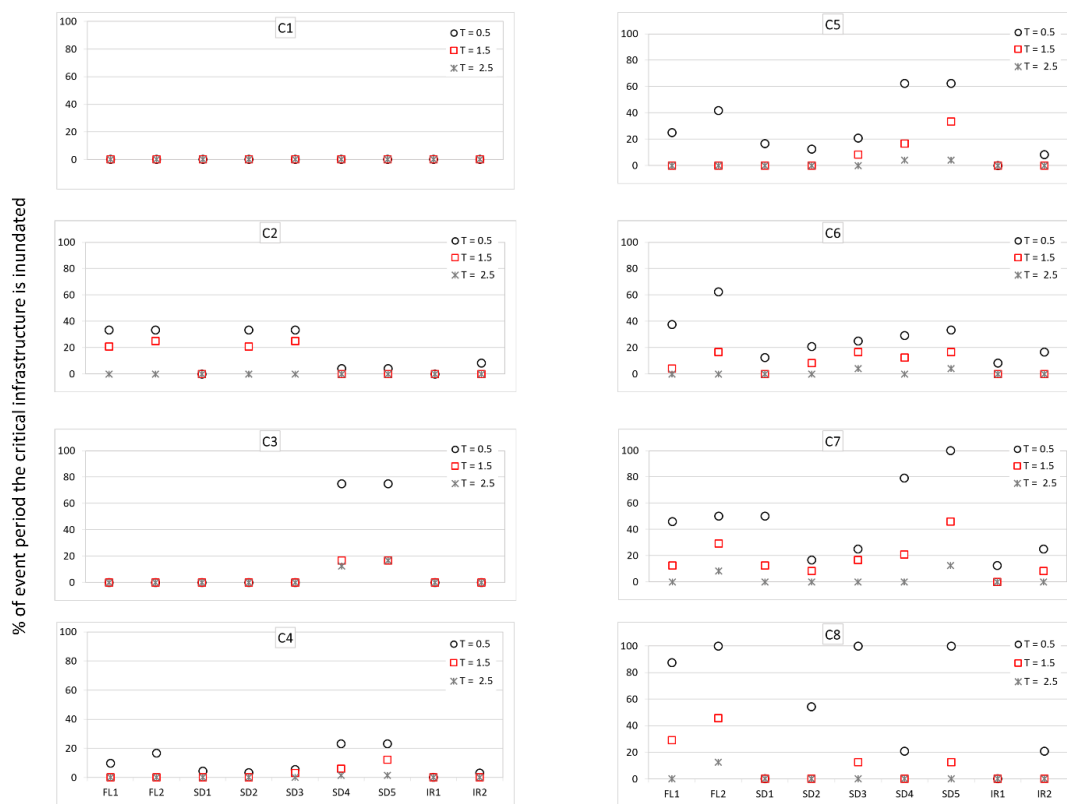
Figure 8: Peak over threshold (T=0.5, 1.5 and 2.5m) at selected critical infrastructures. Hurricanes scenarios, along the x-axis, are labelled according to Table 3 and explained in chapter 2.2. Critical infrastructures are labelled CI1 to CI8, as described in Table 1.

Table 1: Study area- Characteristics of the considered CIs, with river and model domain information. Basin area represents the area of the underlining watershed; domain area is the extent of the simulation domain; reach length represents the length of the stream within the domain; hydrologic distance represents the distance from each CI to the coastline.

Critical Infrastructure (CI)	Town	Rivers	Basin area, km^2	Domain area, km^2	Reach length, km	Hydrologic length, km
CI1	Coscob	Mianus River	216.6	7.5	7.8	4.5
CI2	Southend	Rippowam River	308.4	12.1	4.9	5.3
CI3	Norwalk	Norwalk River	268.7	20.7	8.3	7.8
CI4/ CI5	Branford	Branford River	84.5	7.9	6.7	8.8/5.3
CI6	Guilford	West River	126.4	2.2	3.7	5.1
CI7	Madison	East & Neck Rivers	173.0	8	5.3	6.8
CI8	Stonington	Stonington harbor	10.0	14.9	5.2	2.9

Table 2: Model domain information for Florence

Horizontal Resolution	18, 6, and 2 km
Vertical levels	28
Horizontal Grid Scheme	Arakawa C grid
Nesting	Two-way nesting
Convective parameterization	Grell 3D ensemble scheme (18 and 6 km grids only)
Microphysics option	Thompson graupel scheme (Thompson et al., 2008)
Longwave Radiation option	RRTM scheme (Mlawer et al., 1997)
Shortwave Radiation option	Goddard Shortwave scheme (Chou and Suarez 1994)
Surface-Layer option	Monin-Obukhov Similarity scheme
Land-Surface option	Noah Land-Surface Model (Tewari et al., 2004)
Planetary Boundary Layer	Yonsei scheme (Song–You et al., 2006)

Table 3: Accumulated precipitation & peak flows (with return period reported within brackets) for the simulated events. Recurrence interval (within brackets) and total volume of each event is also shown. Reader should refer to Chapter 2.2 for a detailed description of each hurricane scenario (IR for Irene, SD for Sandy, FL for Florence). Critical infrastructures are labelled CI1 to CI8 according to Table 1.

	Accumulated precipitation (mm)				Peak flow, m^3/s (return period)			
CIs	IR1/IR2	SD1/SD2 /SD3	SD4/SD5	FL1/FL2	IR1/IR2	SD1/SD2 /SD3	SD4/SD5	FL1/FL2
CI1	187.8	24.8	555.3	128.5	158.5(56)	3.4(<2)	242.4(316)	51.3(<2)
CI2	177.8	24.7	546.9	147.5	201.1(58)	9.3(<2)	319.1(326)	87.4(5)
CI3	173.5	21.5	526.8	165.1	126.7 (26)	3.3 (<2)	201.7(28)	74.9(<2)
CI4/ CI5	98.1	17.0	338.2	192.0	93.9(5)	4.7(<2)	178.3(98)	106.1(13)
CI6	91.6	17.7	330.2	203.9	85.7(5)	1.3(<2)	168.4 (48)	113.3(8)
CI7	86.1	15.1	316.6	200.7	93.5(5)	0.9(<2)	197.0(301)	143.2(51)
CI8	58.5	8.9	323.7	289.2	30.8(3)	0.03(<2)	94.7(6)	93.1(6)

Table 4: Maximum total water levels (meter) for tide and surge at the downstream boundary. Reader should refer to Chapter 2.2 for a detailed description of each hurricane scenario (IR for Irene, SD for Sandy, FL for Florence). Critical infrastructures are labelled CI1 to CI8 according to Table 1.

CIs	FL1	FL2	SD1	SD2/ SD4	SD3/ SD5	IR1	IR2
CI1	3.5	4.1	2.8	3.8	4.4	3.1	3.7
CI2	3.5	4.1	2.8	3.8	4.4	3.1	3.7
CI3	3.5	4.1	2.8	3.8	4.4	2.5	3.1
CI4/ CI5	3.5	4.1	2.7	4	4.6	2.5	3.1
CI6	3.4	4.1	2.7	4	4.6	2.5	3.1
CI7	3.5	4.1	2.1	3.1	3.7	2.5	3.1
CI8	3.5	4.1	2.3	2.9	3.5	1.4	2

Table 5: Overall extent of the inundated area (in km^2), and the relative difference (% change in parenthesis) compared to the FEMA 100yr Flood Zone

CIs	FL1	FL2	SD1	SD2	SD3	SD4	SD5	IR1	IR2
CI1	1.6	1.8	0.9	1.4	1.9	1.7	2.0	1.3	1.5
	(-8.5)	(2.9)	(-48.1)	(-21.7)	(8.3)	(-2.8)	(13.9)	(-27.5)	(-15.9)
CI2	3.9	4.0	1.9	2.1	2.3	3.7	4.8	1.6	4.9
	(134.2)	(139.4)	(-12.7)	(25.6)	(36.3)	(123.7)	(185.2)	(-1.9)	(192.2)
CI3	4.7	4.9	3.5	4.0	4.3	5.4	7.1	3.2	4.0
	(2.6)	(7.5)	(-24.5)	(-10.5)	(-6.2)	(17.5)	(56.2)	(-29.3)	(-12.1)
CI4/CI5	2.7	3.2	2.4	2.6	3.4	2.9	3.6	2.0	2.4
	(-8.3)	(8.4)	(-18.5)	(0.3)	(13.8)	(2.5)	(22.2)	(-32.3)	(-17.3)
CI6	0.9	0.9	0.7	0.8	1.0	0.9	1.0	0.7	0.8
	(3.7)	(13.1)	(-14.9)	(-10.3)	(16.6)	(11.4)	(16.5)	(-20.4)	(-4.8)
CI7	2.5	2.7	1.6	2.0	2.6	2.1	2.6	1.9	2.3
	(1.0)	(12.5)	(-33.9)	(-12.8)	(8.5)	(-10.7)	(7.3)	(-23.5)	(-7.5)
CI8	3.1	3.5	0.4	2.1	2.6	2.2	2.7	1.1	1.8
	(4.5)	(18.4)	(-87.8)	(-28.8)	(-11.1)	(-22.3)	(-8.9)	(-63.1)	(-37.9)

Note: (-) Area inundated less than FEMA's 100yr zone